


CFD study on heat transfer augmentation of rectangular shaped pinfin heatsink through the insertion of perforation and bulges

Raduan Rahman Redu^{1*}, Md. As-Ad Adib Rafi^{1*}, Mohammad Rejaul Haque^{1*} , M Merajul Haque²

1 Department of Mechanical and Production Engineering, Ahsanullah University of Science and Technology, Dhaka-1208, Bangladesh.

2 Department of Industrial and Manufacturing Systems Engineering, Iowa State University, Ames, IA 50011, USA

Received November 17, 2021

Revised February 6, 2022

Accepted February 26, 2022

Published online: May 30, 2022

Keywords

Rectangular shaped

Pin fin

Perforation and Bulge

Nusselt number

Pressure drop

Heat transfer enhancement

Abstract: Due to the rapid minimization of electronic gadgets, a significant amount of heat is generated in the electric parts and it becomes a serious concern. Hence, it is necessary to minimize heat to get better performance of the equipment. A numerical investigation is conducted to observe the effect of convective heat transfer enhancement for rectangular shaped pin fin heatsinks. Different shapes of holes in fins and different heights of bulges are added to create more surface area to reduce the excess heat for better performance. The addition of bulge is the novelty of the present work. Hence, a passive cooling technique and staggered arrangement of pin fin have been proposed for a better flow characteristic and heat transfer performance. To predict the turbulent flow parameters, working fluid is modeled using Navier-Stokes's equations and RANS-based k- ϵ turbulent model. The research is carried out utilizing CFD software (COMSOL Multiphysics 5.4) based on the FEM for turbulent flow region. The numerical results show that rectangular-shaped elliptical perforated with a bulge height of 4.5 mm pin fin heatsink, ensuring the highest hydro-thermal performance factor of 1.262 to 1.297 which shows the improvement of around 26% to 29% when compared to previous findings.

© 2022 The authors. Published by Alwaha Scientific Publishing Services, ASPS. This is an open access article under the CC BY license.

1. Introduction

In recent years, the advances in electronic devices having high power result in an excessive heat production issue. Due to the Joule impact's, the excessive heat should be taken out from the chip to keep an efficient performance of these electronic devices without compromising the price. Additionally, the breakdown pace of electronic parts increments significantly with the increase of temperature within the parts. Likewise, the high heat causes breakdown in the bond joints of electronic chips mounted on the circuit board due to excessive temperature variation (Cengel & Heat, 2003). Heatsinks play a crucial part in hardware by cooling optoelectronic gadgets such as higher-power lasers

and light-producing diodes (LEDs) (Oberoi, 2011; Patel & Matawala, 2019). There are countless test, hypothetical, and mathematical examinations have been done about heatsink with heat transfer enhancement. (Soodphakdee, Behnia, & Copeland, 2001) conducted an experimental study and determined the heat transfer of various regularly utilized practical pin fin configurations to limit heat obstruction at restricted airspeeds and pressure drops. They considered plate fins and pin balances of round, square, and circular, and they placed the fins in inline and staggered exhibits. A round exhibit of 1 mm distance across pinfins with a 2 mm pitch was picked for the CFD simulation. To provide a similar wetted zone for every unit volume, the pitch was fixed. The speed of the air was from 0.5 ms⁻¹ to 5

 Corresponding author. E-mail address: md.rejaulh37.mpe@aust.edu – Dr. Mohammad Rejaul Haque, Assistant Professor, MPE, AUST

This work is licensed under a Creative Commons Attribution 4.0. License (CC BY 4.0) <http://creativecommons.org/licenses/by/4.0/>

ENERGY AND THERMOFLUIDS ENGINEERING | ETE | ISSN 2716-8026 (PRINT)

Available online at <https://asps-journals.com/index.php/ete>

<https://doi.org/10.38208/ete.v2i1.348>

ms-1. They discovered that the staggered cases had better heat transfer enhancement and lower pressure than the inline ones. Another study (Sahiti, Durst, & Geremia, 2007) reported that the curved cross-segments offer the best performance. (Chamoli, Chauhan, & Thakur, 2011) studied the heat transfer and friction loss characteristics in a horizontal rectangular channel attached with a circular profile fin. The Reynolds number varied from 5000 to 30000. They studied round profile fin of 5 cm in height and a wide of 2 cm. Reynolds number, fin arrangement, and fin pitch were the considered parameters in their study. The $k-\epsilon$ model was chosen for the simulation as Reynolds number is higher than 2300. (Yousfi, Sahel, & Mellal, 2019) considered the pyramid shape pin fin where they fluctuate the proportion of the pyramid from 0 to 1. From available literatures (Maji, Bhanja, & Patowari, 2017; Maji, Bhanja, Patowari, & Kundu, 2019; Shaeri & Yaghoubi, 2009; Velayati & Yaghoubi, 2005) and others on, a colossal number of trials, hypothetical, and mathematical examinations concerning heat transfer improvement with a modest amount of pressure drop in the heatsink have been done. Furthermore, to compare the outcome, they additionally planned for three different shaped pinfins. They supported the results depending on the simulation (COMSOL Multiphysics 5.4) carried out for Reynolds numbers ranging from 8547 to 21367. They found that for $ROP = 1$, rectangular pin shows the most impressive performance. Also, from available literatures (Chin, Foo, Lai, & Yong, 2013; Maji et al., 2017; Maji et al., 2019; Maradiya, Vadher, & Agarwal, 2018; Mohammed, Gunnasegaran, & Shuaib, 2011; Shaeri & Yaghoubi, 2009) and others on, heat transfer improvement with a modest amount of pressure drop was observed during the implementation of the various heatsink. Absurd heat from microelectronic parts is major for discarding to manufacture the framework's dependability (Ismail, 2013). To improve the cooling execution of the heatsink, holes, for example, tiny channels of square and roundabout cross-areas, are orchestrated alongside fin's length (Ismail, Reza, Zobaer, & Ali, 2013). The convective heat transfer is higher in perforated pin (Baqir, Qasim, & Adnan, 2014). One of the best ways to cool the surface is to arrange the perforated pin fin by staggered arrangement on the heatsink base (Ali & Arshad, 2017; Bilen, Akyol, & Yapici, 2001; Sparrow, Ramsey, & Altemani, 1980). The mathematical and operational boundaries are vital to their cooling execution as heatsinks works in viable applications. (Subramanyam & Crowe, 2000; Yang, Soodphakdee, & Behnia, 2002) reasoned that CFD-based

methodology gives outstanding and reliable data on the performance analysis of heat sinks. The perforation in the pinfins is another design that assists with the decreasing of the stagnated zones of flow behind the pins and therefore enhances the heat transfer co-efficients (Al-Damook, Summers, Kapur, & Thompson, 2016a, 2016b; Al-Sallami, Al-Damook, & Thompson, 2017). Accordingly, compared with the traditional heatsinks, bulges on the heatsink surface can create a significant improvement in the hydrothermal performance of heatsinks (Qi, Zhao, Cui, Chen, & Hu, 2018; Zhao, Guo, Qi, Chen, & Cui, 2019).

In this study, the effects of differently shaped perforated pin fin heatsinks with and without bulges of different heights are analyzed to improve the performance of the pin fin heatsinks. Incompressible air is used as a working fluid. To predict the turbulent flow parameters, working fluid is modeled using the Navier-Stokes's equations and RANS based $k-\epsilon$ turbulent model. The $k-\epsilon$ model was chosen for the simulation as Reynolds number is higher than 2300 as similar to (Chamoli, Chauhan, & Thakur, 2011) and (Yousfi, Sahel, & Mellal, 2019). The investigations are achieved using CFD based FEM solver for the Reynolds number ranging from 8547 to 21367. The newly improved design can be easily understandable when comparing the HTPF with the recent journal (Yousfi, Sahel, & Mellal, 2019). The standard $k-\epsilon$ also presents a robust model from the literature (Kakaç, Shah, & Aung, 1987; Yousfi et al., 2019).

2. Problem Description

In the present study, the computational model dimensions (length, width and height of the heatsink and pin fin) as well as the material were taken from (Yousfi, Sahel, & Mellal, 2019). On the other hand, the present work designs the dimensions of the different shapes of perforation and bulges. For material, aluminium is utilized to construct the rectangular shape pin fin heatsink, because it is the second most malleable metal and the sixth most ductile material. Moreover, it has low density, nontoxic, has a high thermal conductivity, has excellent corrosion resistance and can be easily cast, machined and formed. In Fig. 1, the distinctive heatsink setups present the base-plate having dimensions $W_c \times L_c$ (100 mm \times 100 mm). On the base plate, a rectangular shape of pin fin was taken. The rectangular shape fins having measurements $W_f \times L_f$ which is illustrated in Fig. 2(a). From Fig. 2(b-e), four distinct variations of the perforations (rectangular, circular, hexagonal and elliptical) are considered with the same peripheral areas. Every one of the outskirts is put the same as rectangular ($W_p \times L_p$). From

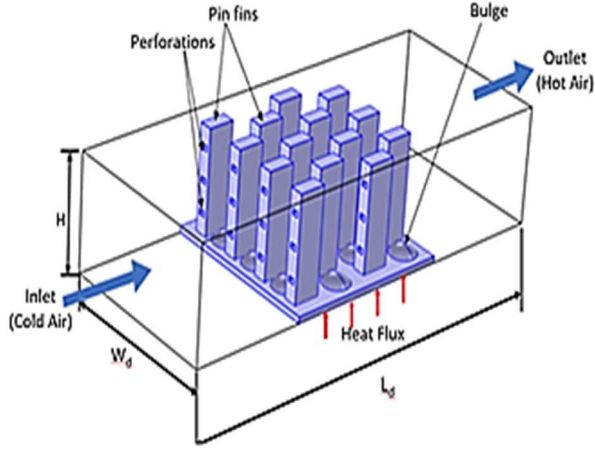


Fig. 1. Schematic diagram of the computational domain.

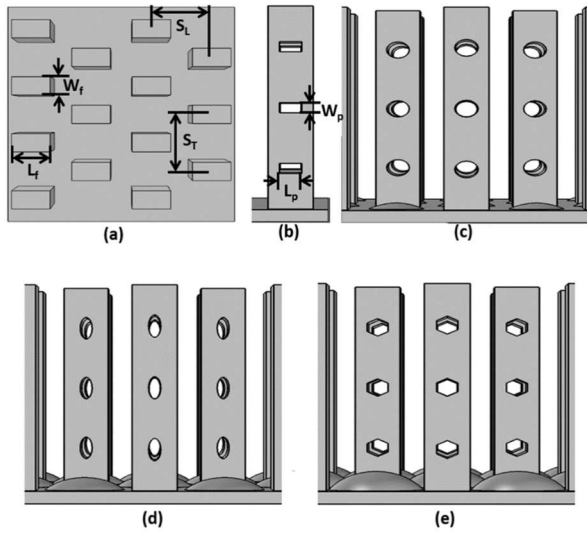


Fig. 2. (a) Rectangular pin fin, (b) rectangular perforation, (c) circular perforation with bulge height of 1.5 mm, (d) elliptical perforation with bulge height of 3 mm, (e) hexagonal perforation with a bulge height of 4.5 mm.

Fig. 2(c-e), three distinct heights (1.5 mm, 3 mm and 4.5 mm) of bulges over the base plate of heatsinks are considered. The distance between the center to center of the pin fins is pitch length (S_L). The pin fins are arranged in a staggered arrangement over the base plate for all the configurations and taken S_T as the transverse pitch length. The heatsink is placed into the center of a rectangular computational domain having dimensions $W_d \times L_d$ which is illustrated in Fig. 1. Dimensions of pin fin heatsinks configurations are given in Table 1.

Table 1. Dimensions of pinfin heatsinks configurations.

H (mm)	H _p (mm)	W _d (mm)	L _d (mm)	W _f (mm)	L _f (mm)
5	50	100	240	8	16

W _p (mm)	L _p (mm)	S _L (mm)	S _T (mm)	t (mm)
2.5	4	25	25	3

2.1 Governing Equations

In CFD simulation continuity, momentum, and energy equations are applied to govern the turbulent flow, incompressible air flow, and heat transfer through the pin fin heat sink. At steady-state conditions, the governing equations are disclosed as follow-

Continuity equation,

$$\frac{\partial u}{\partial x} + \frac{\partial v}{\partial y} + \frac{\partial w}{\partial z} = 0 \quad (1)$$

Momentum equations, X-Momentum:

$$\rho \left[u \frac{\partial u}{\partial x} + v \frac{\partial u}{\partial y} + w \frac{\partial u}{\partial z} \right] = -\frac{\partial p}{\partial x} + \mu \left[\frac{\partial^2 u}{\partial x^2} + \frac{\partial^2 u}{\partial y^2} + \frac{\partial^2 u}{\partial z^2} \right] \quad (2)$$

Y-Momentum:

$$\rho \left[u \frac{\partial u}{\partial x} + v \frac{\partial u}{\partial y} + w \frac{\partial u}{\partial z} \right] = -\frac{\partial p}{\partial x} + \mu \left[\frac{\partial^2 u}{\partial x^2} + \frac{\partial^2 u}{\partial y^2} + \frac{\partial^2 u}{\partial z^2} \right] \quad (3)$$

Z-Momentum:

$$\rho \left[u \frac{\partial w}{\partial x} + v \frac{\partial w}{\partial y} + w \frac{\partial w}{\partial z} \right] = -\frac{\partial p}{\partial x} + \mu \left[\frac{\partial^2 w}{\partial x^2} + \frac{\partial^2 w}{\partial y^2} + \frac{\partial^2 w}{\partial z^2} \right] \quad (4)$$

Energy equation:

$$u \frac{\partial T}{\partial x} + v \frac{\partial T}{\partial y} + w \frac{\partial T}{\partial z} = \frac{k_f}{\rho C_p} \left[\frac{\partial^2 T}{\partial x^2} + \frac{\partial^2 T}{\partial y^2} + \frac{\partial^2 T}{\partial z^2} \right] \quad (5)$$

For the present simulation, the k-ε standard turbulence model is utilized. This model is used mainly in writing to foresee the violent streams in channel-fitted impediments (Sahel, Ameer, Benzeguir, & Kamla, 2016) as similar to the calculations investigated in the current investigation. The k-ε standard model depends on the energy scattering ε, Eq. (6) and the fierce motor energy, k Eq. (7).

$$\rho(u \cdot \nabla) \varepsilon = \nabla \left[\left(\mu + \frac{\mu T}{\sigma \varepsilon} \right) \nabla \varepsilon \right] + C_{sl} \frac{\varepsilon}{k} P_k - C_{cl} \rho \frac{\varepsilon^2}{k}, \varepsilon = \varepsilon p \quad (6)$$

$$\rho(u \cdot \nabla) k = \nabla \left[\left(\mu + \frac{\mu T}{\sigma \varepsilon} \right) \nabla k \right] + P_k - \rho \varepsilon \quad (7)$$

where the production term is given Eq. (8) as follow:

$$P_k = \mu_T [\nabla u : (\nabla u + (\nabla u)^T)] \quad (8)$$

The turbulent viscosity is modeled in Eq. (9) as:

$$\mu_t = \rho C_\mu \frac{k^2}{\varepsilon} \quad (9)$$

The empirical constants for the standard k-ε model are given as follow (Eq. (10)),

$$\Delta P = P_{In} - P_{Out} \quad (10)$$

where, P_{In} is the inlet pressure and P_{Out} is the outlet pressure of the channel. The thermal resistance (R_{th}) in Eq. (11) is calculated as follow (Yousfi et al., 2019):

$$R_{th} = \frac{T_w - T_{in}}{q''} \quad (11)$$

where, T_w and T_{in} are the average wall temperature and air inlet temperature respectively. Besides, q'' is the heat flux applied to the base plate. The Reynolds number (Re) is expressed in Eq. (12) as (Yousfi et al., 2019)

$$R_e = \frac{\rho_{Air} v D_h}{\mu_{Air}} \quad (12)$$

where, ρ_{Air} is the density of air, D_h is the hydraulic diameter of the channel, μ_{Air} and v are the dynamic viscosity of air and the mean air inlet velocity, respectively.

Nusselt number (Nu) is considered to determine the convection heat transfer coefficient inside the channel given in Eq. (13) (Yousfi et al., 2019):

$$Nu = \frac{q'' D_h}{k_{Air} (T_w - \frac{T_{Out} + T_{In}}{2})} \quad (13)$$

where, T_{In} , T_{Out} and T_w are the temperature of airflow at the inlet, the outlet of the channel, and the mean temperature of the heated surface, which is in contact with the airflow. The q'' is the heat flux, which is kept as 5903 Wm^{-2} consistent with previous work (Chin et al., 2013; Yousfi et al., 2019).

The effectiveness of the designed fins for improving the heat transfer enhancement can be assessed by the hydro-thermal performance factor (HTPF) which is the ratio of the relative effect of change in Nusselt number to the change in pressure drop. Hydro-Thermal Performance Factor (HTPF) presented in Eq. (14) (Yousfi et al., 2019) is considered as the key parameter to evaluate the overall performance of the newly designed pin fin heatsinks. It gives an evaluation of heat transfer with the expense of pressure drop.

$$HTPF = \frac{(Nu_{Pins} / Nu_{Rectangular})}{(\Delta P_{Pins} / \Delta P_{Rectangular})^{1/3}} \quad (14)$$

3. Numerical Model

3.1 Boundary Condition

In CFD, the discretized governing equations are solved iteratively with the incorporation of appropriate Boundary conditions. Different Boundary conditions used for the present analysis are given below as shown in Table 2.

Table 2. Boundary conditions for the computational domain.

Boundary Name	Condition	Energy
Inlet	Momentum Fully Developed velocity at inlet, u (ms^{-1})	Room Temperature, $T_{in} = 293.15 K$
Wall	No slip	Adiabatic
Outlet	Pressure, $P_{out} = 0.00 Pa$	
Turbulent Model	$k - \varepsilon$ model	
Coolant	Air (incompressible fluid)	
Material	Aluminum A5083 (Thermal Conductivity, $k_m = 167 Wm^{-1}K^{-1}$)	
Heat sink	Heat Flux, $q'' = 5903 Wm^{-2}$	

3.2 Mesh selection and solver settings

COMSOL Multiphysics 5.4, a commercial FEM solver is used to run the simulations for the present investigation. After the import of variously modeled heat sink from CAD software, the whole computational domain is meshed by exploiting the tetrahedral network option from the solver as shown in Fig. 3. The total number of elements are considered as 1873367, 2150870, 2674966, 3171664 to run the grid independency test. Simulations are tried for rectangular perforated pin fins with these number of mesh elements, where the deviation of the results of temperature gradient magnitude was found to be less than 0.012% between the 3000000 and 3200000 mesh elements as shown in Fig. 4.

To solve the governing equation, the segregated solvers with the Generalized Minimal Residual (GMRES) iterative methods are applied. A number of 20 and 0.01 factor error and tolerance are used respectively. In order to accelerate the process, the geometric multi-grid solver is used with the pre-conditioner Parallel Sparse Direct Linear Solver (PARDISO). The simulations ran on PC-i7 with a computer

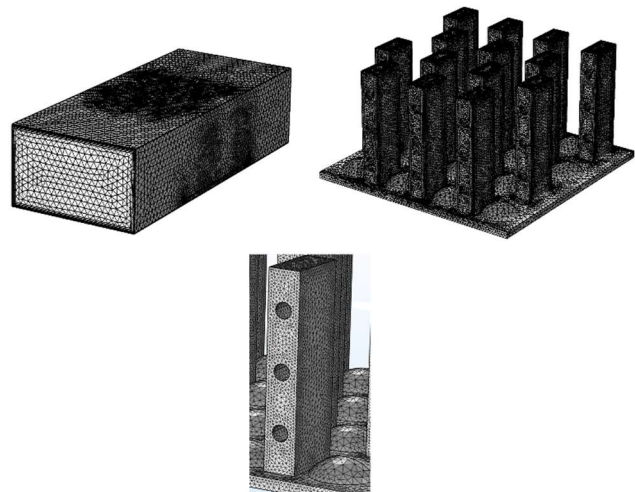


Fig. 3. Sample meshing of the domain.

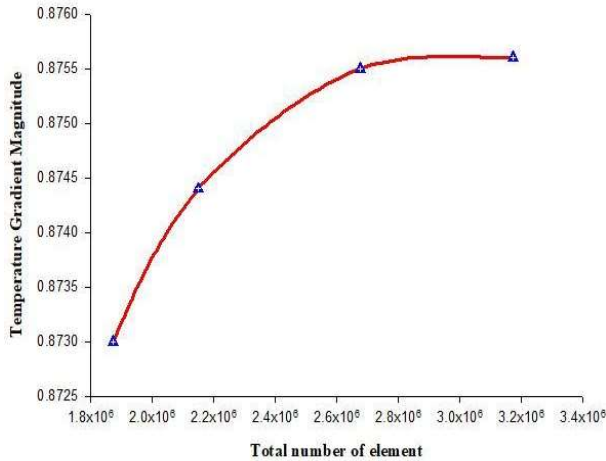


Fig. 4. Grid independence test.

chip frequency of 4.1, and a RAM of 16GB. A standard running time for the estimation of an arbitrary case is around seven hours to seventeen hours based on different geometry.

4. Results

4.1 Validation of the Numerical Model

After the mesh independency test, the present scheme is well validated with respect to previous literature. The heat transfer and flow behaviors are analogized with previous numerical work (Yousfi et al., 2019). The current investigation plots the results of Nusselt number and pressure drop for square and rectangular shape pin fin heatsinks with the same geometrical and thermophysical properties of Yousfi et al., 2019 as shown in Figs. 5 and 6.

Both of the considered figures show a favorable agreement between the present numerical results and the considered literature (Yousfi et al., 2019) results. The Nusselt number (Nu) deviation is found to be varied between 0.69% to

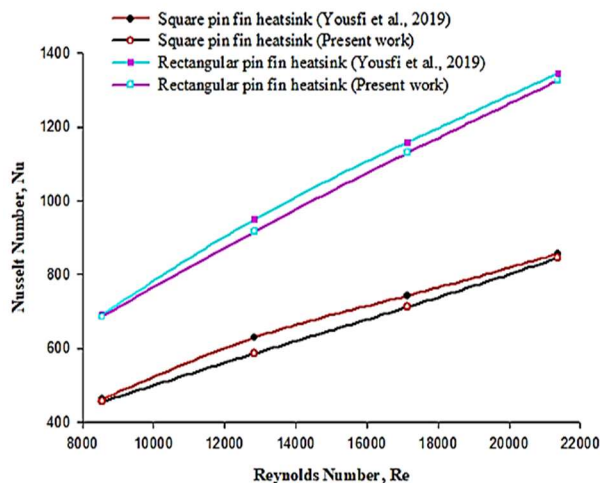


Fig. 5. Comparison of Nusselt number (Nu) results.

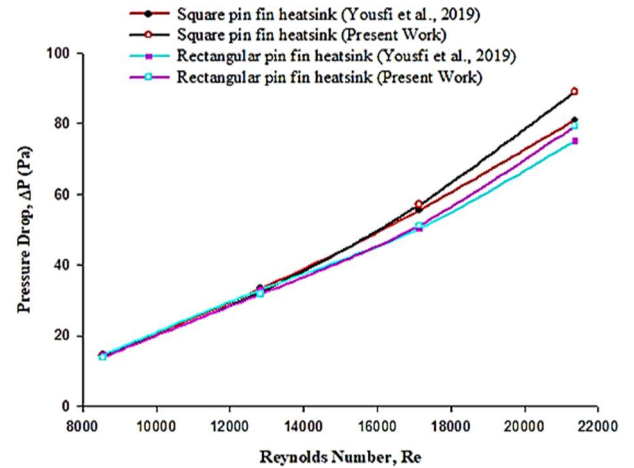


Fig. 6. Comparison of pressure drop (ΔP) results.

6.88% for square and rectangular shape pin fin heatsink. Hence, the present numerical scheme is a well reasonable presentation of an earlier numerical work of (Yousfi et al., 2019) indicating the relevance of the present model.

4.2 Effect of Reynolds Number (Re) on heat transfer

From Fig. 7, it is quite noticeable that increasing the Reynolds number enhances the heat transfer. The highly concentrated heated zone (yellow region) is observed at $Re = 8547$ as shown in Fig. 7. As Reynolds number gradually increases from 8547, the yellow regions shift to a more intense color region of lower temperature for subsequent all the Reynolds numbers as observed from Fig. 7 ($Re=12830$ to $Re=21367$). The lowest average temperature for heatsink fin combination is observed for $Re=21367$, indicating the higher the turbulence effect, the higher the mixing resulting better heat transfer performance.

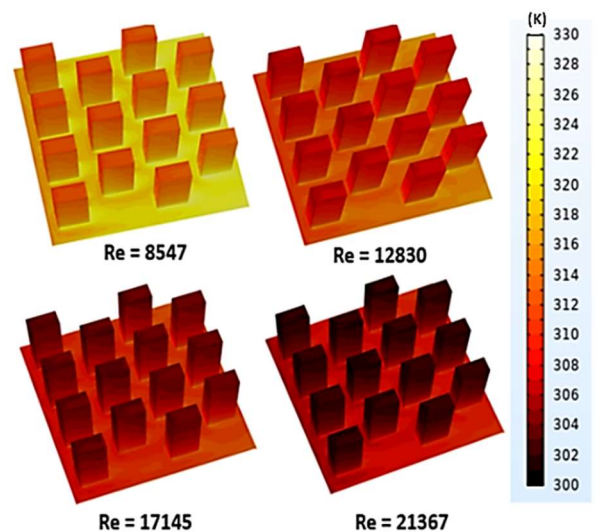


Fig. 7. 3D temperature contour plots for different Reynolds number of perforated rectangular shape pin fin heatsink.

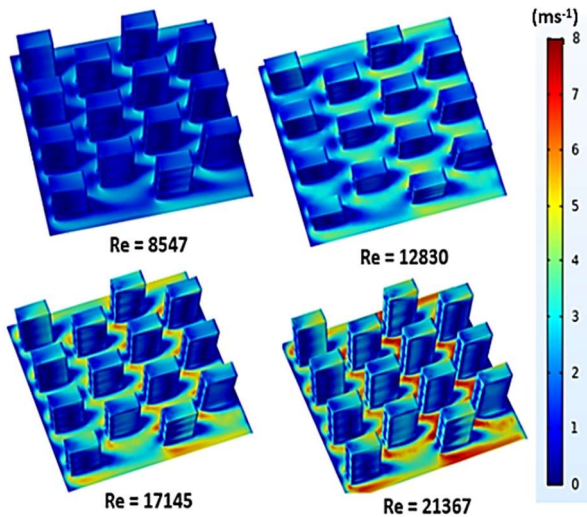


Fig. 8. 3D velocity magnitude contour plots for different Reynolds numbers of perforated rectangular shape pin fin heatsink.

From the velocity magnitude contour plots (Fig. 8), it is comprehensible that the establishment of recirculation zones (blue color) of the pin fins airflow downstream appears for all the cases. But, these zones (blue colour) begin to disappear following the increase of Reynolds number ranging from 8547 to 21367. On the other hand, the reattachment zones (red colour) begin to appear according to the increase of Reynolds number from 8547 to 21367. However, highest velocity area is observed for higher Reynolds numbers (for $Re=17145$, yellow color and for $Re=21367$, red color).

4.3 Effect of Perforation shape on heat transfer

The temperature distribution for 4-different perforation shapes has been illustrated in Fig. 9. In Fig. 9, the density of

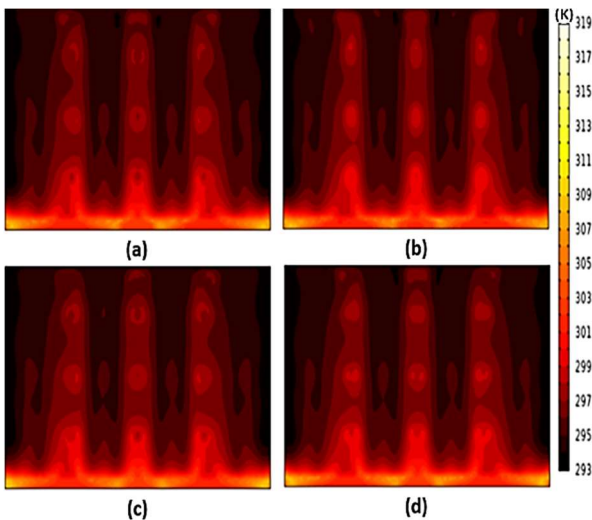


Fig. 9. 2D temperature contour plots (at $X=50.01$ mm from YZ plane) for (a) circular, (b) elliptical, (c) hexagonal, (d) rectangular perforated pin fin heatsink at $Re=21367$.

the yellow region is changing slightly for different shapes of perforations. The heat transfer is maximum for circular and elliptical perforations, though the circular perforations are marginally better. The base-plate temperature for circular and elliptical shapes perforated heatsinks are around 303 K to 305 K, and the pin fin temperature varies from 298 K to 301 K. Moreover, for rectangular and hexagonal shaped perforated heatsinks, the temperature of base-plates is around 308 K to 310 K and 307 K to 309 K respectively, and the circular and elliptical perforated pin fin heatsinks temperature varies from 299 K to 302 K and from 299 K to 301 K respectively.

4.4 Effect of Bulges on heat transfer

Increasing the bulge height and area as shown in Figs. 10-12, flow pattern through the interspace of the pin fin changes that creates a more favorable condition for the enhancement of heat transfer. In Fig. 10(b), where bulge height is 1.5 mm, flow is taking a diverging route after passing the bulges.

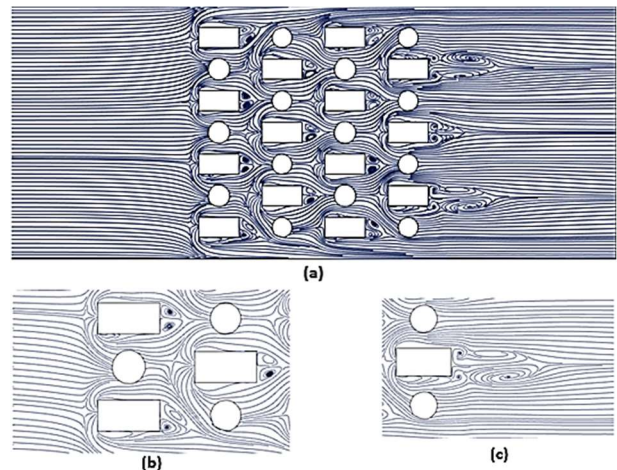


Fig. 10. (a) Streamline plots for 1.5 mm bulge height, (b) entry region, (c) end region.

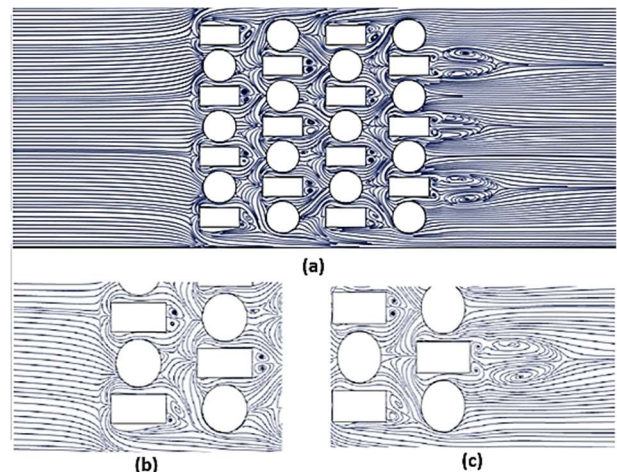


Fig. 11. (a) Streamline plots for 3 mm bulge height, (b) entry region, (c) end region.

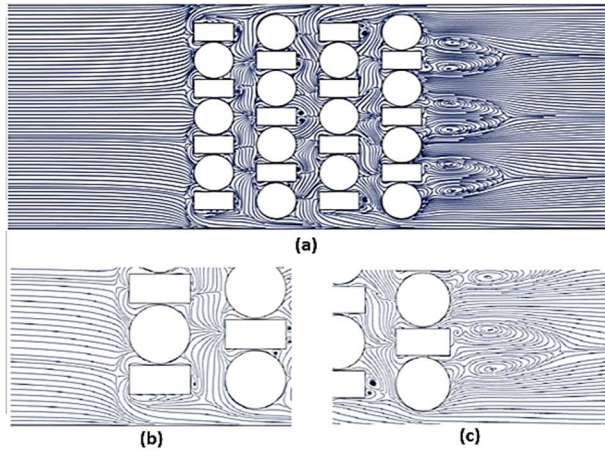


Figure 12. (a) Streamline plots for 4.5 mm bulge height, (b) entry region, (c) end region.

Hence, heat transfer contact area decreases, reducing heat transfer compared to $h=4.5$ mm (Fig. 12(b)) where the increased bulge height and surface area directs the flow to a converging route towards the next array of fin of the heatsink causing higher frontal area contact and thereby enhances the heat transfer. From Fig. 10(c)-12(c), it is understandable that by increasing the bulge height and surface area; there are more vortexes at the end of the array of the fin. This vortex plays a vital role in mixing the fluid with the last array of fin before leaving the domain. Hence, subsequent heat transfer is possible due to this end mixing mechanism. However, the pressure differences are also higher for bulges compared to ones without bulges. Hence, more pumping power is required thereby affecting the overall performance.

4.5 Effect of Reynolds number on Nusselt number

From Fig. 13, the Nusselt number rises almost linearly with the increment of the Reynolds number for all the configurations, the rectangular shaped elliptical perforation pin fin heatsinks with a bulge height of 4.5 mm has the maximum Nusselt number compared to all other cases. However, the calculated enhancement of Nu is 24.6% at $Re=8547$ and 26.6% at $Re=21367$ compared to the corresponding rectangular shaped fin respectively. However, the rate of increment of heat transfer is also higher at a higher Reynolds number.

4.6 Effect of Reynolds number on HTPF

Fig. 14 shows that the HTPF values are increasing with the increase of Re number. The HTPF evaluated from eq. (14) has unit value for the solid rectangular pin fin heatsink design which is our baseline case adopted from the previous literature (Yousfi et al., 2019). However, from Fig. 14, the rectangular pin fin elliptical perforation bulge height of

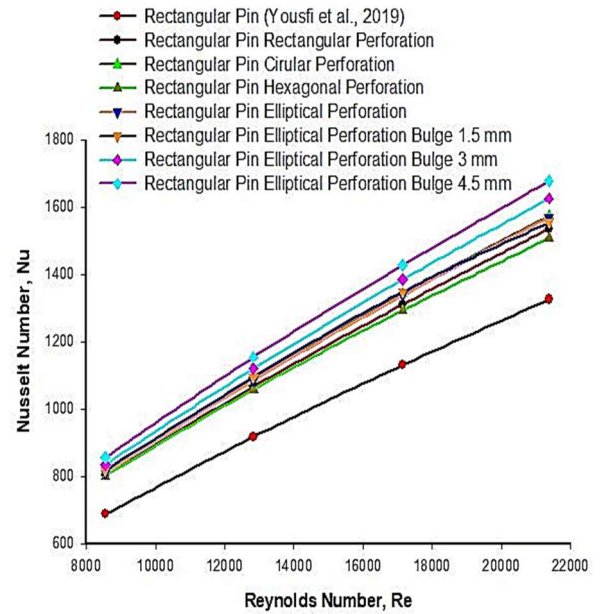


Fig. 13. Variation of Nusselt number (Nu) with Reynolds number (Re) for different cases.

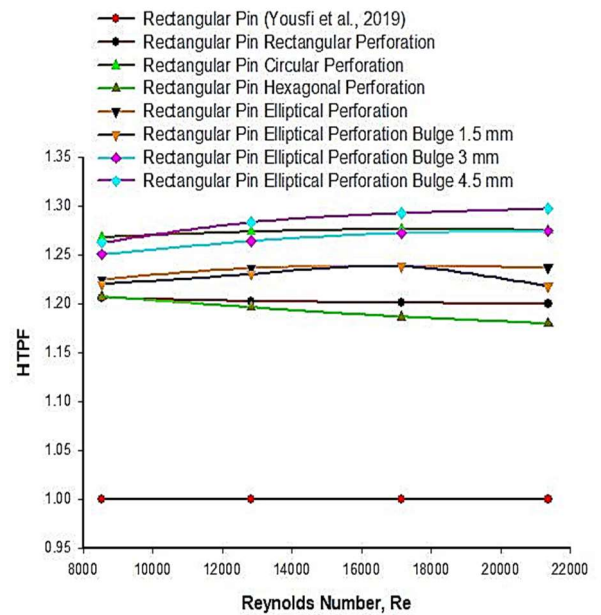


Fig. 14. Variation of HTPF with Reynolds number (Re) for different cases.

4.5mm depicts the highest value of HTPF for higher Reynolds numbers. So, for the present study, the rectangular pin fin elliptical perforation bulge height of 4.5 mm merits to consider in the future CPU heatsink design.

4.7 Effect of Thermal resistance on Pressure drop

Thermal resistance is the ratio of the temperature difference between two surfaces to the heat flow rate per unit area. On the other hand, the larger the pressure loss, the larger the heat flow and the lower the thermal resistance. In Fig. 15, it is observed that thermal resistance

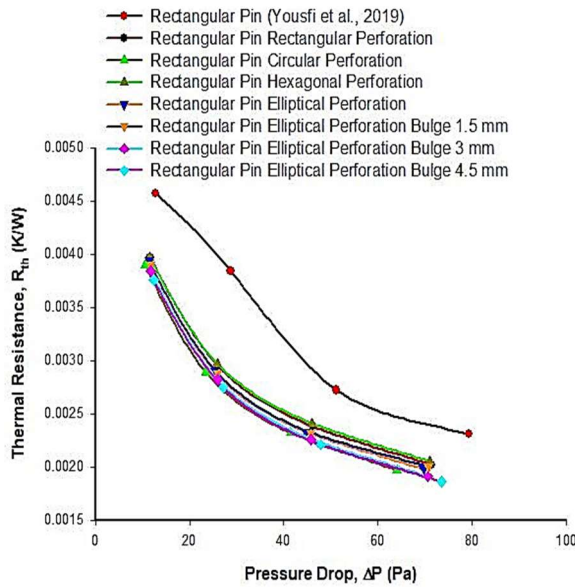


Fig. 15. Variation of thermal resistance (R_{th}) with pressure drop (ΔP) for different cases.

is decreasing by the increasing of the pressure drop. It is known that thermal resistance is inversely proportional to heat transfer, and on the other hand, HTPF is dependent on pressure drop. A higher-pressure drop is the reason for lower HTPF. Also, the pressure drop is lower for the rectangular shaped circular perforation pin fin heatsinks compared to the other cases. Again, for thermal resistance, rectangular pin elliptical perforation with 4.5 mm bulge pin fin has lower values compared to others. If hydro-thermal performance factor (HTPF) is considered as the high priority in heatsink design, then rectangular pin elliptical perforation bulge 4.5 mm pin fin heatsink would be the best possible design under the present consideration.

5. Conclusion

In the present study, 3D CFD simulations are performed in a fully developed steady-state condition where the fluid flow is in turbulent condition. Nusselt number, pressure drop, thermal resistance, as well as HTPF are compared with various design geometries of staggered fin arrangement. The perforation and bulges on the base plate of the heatsinks alters the flow pattern around the pinfins of the heatsink and hence the obtained results clarify the enhancement in both the thermal and hydrothermal performance of the heatsinks. Rectangular shaped elliptical perforation with a bulge height of 4.5 mm ensures the highest possible HTPF. HTPF increases around 26.24% to 29.7% by changing the Reynolds number from 8547 to 21367. From the present study, the obtained Nusselt number (1677.2434) at $Re=21367$ and the HTPF (1.297) is very high compared to previously published cases. Hence,

this design can be more compatible and integration can be done with the possible mode of applications in electronic cooling.

Disclosures

Free Access to this article is sponsored by SARL ALPHA CRISTO INDUSTRIAL.

Acknowledgments

The authors would like to acknowledge the computer facility provided by the simulation lab of the Mechanical and Production Engineering Department of Ahsanullah University of Science and Technology, Dhaka.

All the star (*) marked authors contributed equally to the manuscript and there is no conflict of interest to report.

Nomenclature

Symbol

A	Surface area, mm^2
H	Domain height, mm
h	Conductive heat transfer co-efficient, $\text{Wm}^{-1}\text{K}^{-1}$
k	Thermal conductivity, $\text{Wm}^{-1}\text{K}^{-1}$
T	Temperature, K
q''	Heat flux, Wm^{-2}
v	Inlet air velocity, ms^{-1}
ΔP	Pressure drop, Pa

Subscript

A_b	Base-plate surface area, mm^2
A_d	Domain surface area, mm^2
D_h	Hydraulic diameter, mm
H_p	Fin height, mm
k_{Air}	Thermal conductivity of air, $\text{Wm}^{-1}\text{K}^{-1}$
k_m	Thermal conductivity of aluminum, $\text{Wm}^{-1}\text{K}^{-1}$
L_c	Chip length, mm
L_d	Domain length, mm
L_f	Pin fin length, mm
L_p	Perforation length, mm
P_{In}	Inlet pressure, Pa
P_{Out}	Outlet pressure, Pa
R_{th}	Thermal resistance, KW^{-1}
S_L	Pitch length, mm
S_T	Pitch transverse length, mm
T_{In}	Inlet temperature, K
T_{Out}	Outlet temperature, K
T_w	Average wall temperature, K
W_c	Base-plate width, mm
W_d	Domain width, mm
W_f	Pin fin width, mm

W_p Perforation width, mm

Greek Letter

ρ Density, Kgm^{-3}

ρ_{Air} Density of air, Kgm^{-3}

μ Viscosity, $Kgm^{-1}s^{-1}$

μ_{Air} Viscosity of air, $Kgm^{-1}s^{-1}$

Abbreviation

HTPF Hydro- Thermal Performance Factor

GMRES Generalized Minimal Residual Iterative Methods

CFD Computational Fluid Dynamics

FEM Finite Element Method

Nu Nusselt number

Re Reynolds number

References

- Ali, H. M., & Arshad, A. (2017). Experimental investigation of n-eicosane based circular pin-fin heat sinks for passive cooling of electronic devices. *International Journal of Heat and Mass Transfer*, 112, 649-661.
- Al-Damook, A., Summers, J., Kapur, N., & Thompson, H. (2016a). Effect of different perforations shapes on the thermal-hydraulic performance of perforated pinned heat sinks. *Journal of Multidisciplinary Engineering Science and Technology (JMEST)*, 3(4), 4466-4474.
- Al-Damook, A., Summers, J., Kapur, N., & Thompson, H. (2016b). Effect of temperature-dependent air properties on the accuracy of numerical simulations of thermal airflows over pinned heat sinks, *International Communications in Heat and Mass Transfer*, 78, 163-167.
- Al-Sallami, W., Al-Damook, A., & Thompson, H. (2017). A numerical investigation of the thermal-hydraulic characteristics of perforated plate fin heat sinks. *International Journal of Thermal Sciences*, 121, 266-277.
- Baqir, A. S., Qasim, A., & Adnan, A. (2014). Experimental Study for Staggered Perforated Array of Pins Like Fins in a Rectangular Air Cross Flow. *The Iraqi Journal for Mechanical and Material Engineering*, 14(2), 261-275.
- Bilen, K., Akyol, U., & Yapici, S. (2001). Heat transfer and friction correlations and thermal performance analysis for a finned surface. *Energy Conversion and Management*, 42(9), 1071-1083.
- Cengel, Y., & Heat, T. M. (2003). *A practical approach*: New York, NY, USA: McGraw-Hill.
- Chamoli, S., Chauhan, R., & Thakur, N. (2011). Numerical analysis of heat transfer and thermal performance analysis of surface with circular profile fins. *International journal of energy science*, 1, 11-18.
- Chin, S.-B., Foo, J.-J., Lai, Y.-L., & Yong, T. K.-K. (2013). Forced convective heat transfer enhancement with perforated pin fins. *Heat and Mass Transfer*, 49(10), 1447-1458.
- Ismail, M. F. (2013). Effects of perforations on the thermal and fluid dynamic performance of a heat exchanger. *IEEE Transactions on Components, Packaging and Manufacturing Technology*, 3(7), 1178-1185.
- Ismail, M. F., Reza, M., Zobaer, M., & Ali, M. (2013). Numerical investigation of turbulent heat convection from solid and longitudinally perforated rectangular fins. *Procedia Engineering*, 56, 497-502.
- Kakaç, S., Shah, R. K., & Aung, W. (1987). *Handbook of single-phase convective heat transfer*. John Wiley and Sons Inc., United States : 18 (2), 900 p.
- Maji, A., Bhanja, D., & Patowari, P. K. (2017). Numerical investigation on heat transfer enhancement of heat sink using perforated pin fins with inline and staggered arrangement. *Applied Thermal Engineering*, 125, 596-616.
- Maji, A., Bhanja, D., Patowari, P. K., & Kundu, B. (2019). Thermal analysis for heat transfer enhancement in perforated pin fins of various shapes with staggered arrays. *Heat Transfer Engineering*, 40(3-4), 295-319.
- Maradiya, C., Vadher, J., & Agarwal, R. (2018). The heat transfer enhancement techniques and their thermal performance factor. *Beni-Suef University Journal of Basic and Applied Sciences*, 7(1), 1-21.
- Mohammed, H., Gunnasegaran, P., & Shuaib, N. (2011). Numerical simulation of heat transfer enhancement in wavy microchannel heat sink. *International Communications in Heat and Mass Transfer*, 38(1), 63-68.
- Oberoi, A. S. (2011). Analysis of Heat Transfer Through Perforated Plate Heat Sink. *The IUP Journal of Mechanical Engineering*, 4(4), 55-63.
- Patel, H., & Matawala, V. (2019). Performance Evaluation and parametric optimization of a Heat Sink for Cooling of Electronic Devices with Entropy Generation Minimization. *European Journal of Sustainable Development Research*, 3(4), em0100.
- Qi, C., Zhao, N., Cui, X., Chen, T., & Hu, J. (2018). Effects of half spherical bulges on heat transfer characteristics of CPU cooled by TiO₂-water nanofluids. *International Journal of Heat and Mass Transfer*, 123, 320-330.
- Sahel, D., Ameer, H., Benzeguir, R., & Kamla, Y. (2016). Enhancement of heat transfer in a rectangular channel with perforated baffles. *Applied Thermal Engineering*, 101, 156-164.
- Shaeri, M., & Yaghoubi, M. (2009). Numerical analysis of turbulent convection heat transfer from an array of perforated fins. *International journal of heat and fluid flow*, 30(2), 218-228.

- Sahiti, N., Durst, F., & Geremia, P. (2007). Selection and optimization of pin cross-sections for electronics cooling. *Applied Thermal Engineering*, 27(1), 111-119.
- Shaeri, M., & Yaghoubi, M. (2009). Numerical analysis of turbulent convection heat transfer from an array of perforated fins. *International journal of heat and fluid flow*, 30(2), 218-228.
- Soodphakdee, D., Behnia, M., & Copeland, D. W. (2001). A comparison of fin geometries for heatsinks in laminar forced convection : Part I-round, elliptical, and plate fins in staggered and in-line configurations. *The International Journal of Microcircuits and Electronic Packaging*, 24(1), 68-76.
- Sparrow, E. M., Ramsey, J., & Altemani, C. (1980). Experiments on in-line pin fin arrays and performance comparisons with staggered arrays. *Journal of Heat Transfer*, 102(1), 44-50.
- Subramanyam, S., & Crowe, K. E. (2000). Rapid design of heat sinks for electronic cooling using computational and experimental tools. Paper presented at the Sixteenth Annual IEEE Semiconductor Thermal Measurement and Management Symposium (Cat. No. 00CH37068).
- Yang, J., Soodphakdee, D., & Behnia, M. (2002). Correlations based on CFD and their applications in optimization for staggered and parallel plate fin heatsinks. *Journal of University of Science and Technology Beijing : Mineral Metallurgy Materials (Eng Ed)*, 9(1), 25-30.
- Velayati, E., & Yaghoubi, M. (2005). Numerical study of convective heat transfer from an array of parallel bluff plates. *International journal of heat and fluid flow*, 26(1), 80-91.
- Yousfi, A., Sahel, D., & Mellal, M. (2019). Effects of A Pyramidal Pin Fins on CPU Heat Sink Performances. *Journal of Advanced Research in Fluid Mechanics and Thermal Sciences*, 63(2), 260-273.
- Zhao, N., Guo, L., Qi, C., Chen, T., & Cui, X. (2019). Experimental study on thermo-hydraulic performance of nanofluids in CPU heat sink with rectangular grooves and cylindrical bugles based on exergy efficiency. *Energy Conversion and Management*, 181, 235-246